SGK regulates pH increase and cyclin B-Cdk1 activation to resume meiosis in starfish ovarian oocytes

Enako Hosoda[1], Daisaku Hiraoka[2], Noritaka Hirohashi[1,3], Saki Omi[1], Takeo Kishimoto[2], and Kazuyoshi Chiba[1*]

[1]Department of Biological Sciences, Ochanomizu University, Tokyo 112-8610, Japan.

[2]Science & Education Center, Ochanomizu University, Tokyo 112-8610, Japan.

[3] Present address; Oki Marine Biological Station, Education and Research Center for Biological Resources, Shimane 685-0024, Japan

Running title: SGK-dependent oocyte maturation in ovarian oocytes

This manuscript is uploaded to a preprint server bioRxiv (doi: https://doi.org/10.1101/499699).

[*]Correspondence to:

Kazuyoshi Chiba: E-mail: chiba.kazuyoshi@ocha.ac.jp, Tel: +81-3-5978-5370

Abstract

Tight regulation of intracellular pH (pH_i) is essential for biological processes. Fully-grown oocytes, having a large nucleus called the germinal vesicle, arrest at meiotic prophase-I. Upon hormonal stimulus, oocytes resume meiosis to acquire fertilizability. At this time, pH_i increases through Na^+/H^+ exchanger activity. However, regulation and function of this change remains obscure. Here we show that in starfish oocytes, serum- and glucocorticoid-regulated kinase (SGK) is activated by the PI3K/TORC2/PDK1 signaling after hormonal stimulus, and is required for the pH_i increase and cyclin B–Cdk1 activation. Furthermore, when we clamped pH_i at 6.7, corresponding to the pH_i of unstimulated ovarian oocytes, hormonal stimulus normally induced cyclin B–Cdk1 activation; thereafter, oocytes initiated germinal vesicle breakdown (GVBD), but failed to complete it. Thus, SGK-dependent pH_i increase is likely prerequisite for completion of GVBD in ovarian oocytes. We propose a model that SGK drives meiotic resumption through concomitant regulation of pH_i and the cell-cycle machinery.

33 **Introduction**

34 Intracellular pH (pH_i) is tightly regulated in living cells. Increases in pH_i are required for a variety of
35 physiological and pathological processes, including early embryonic development[1,2,3] and cancer cell
36 survival[4]. A key pH_i regulator, the sodium–proton exchanger (NHE) is a 12-transmembrane protein
37 that increases pH_i by exporting intracellular H^+ and importing extracellular Na^+ (ref. [5]). Many kinases,
38 including serum- and glucocorticoid-regulated kinase (SGK)[6-8], p90RSK[9], and p38MAPK[10,11],
39 activate NHE in mammalian cells.

40 An NHE-dependent pH_i increase has also been reported during oocyte maturation[12-17], a
41 fundamental process involved in the generation of fertilizable eggs, although the underlying
42 regulatory mechanism and function of pH_i increase during oocyte maturation are not completely
43 understood. In the ovaries of most animals, fully-grown oocytes, which have a large nucleus called
44 the germinal vesicle (GV), are arrested at prophase of meiosis I (ProI)[18]. Upon extracellular stimuli
45 by maturation-inducing hormones, ovarian oocytes resume the meiotic cell cycle via activation of
46 cyclin B–Cdk1 and subsequently undergo germinal vesicle breakdown (GVBD)[19-21]. Subsequently,
47 oocytes undergo another arrest at the metaphase of meiosis I or II (MI or MII arrest) that enables
48 successful fertilization[22]. Starfish oocytes have been used as a model to study oocyte maturation for
49 more than half a century[23]. Previously, we reported that pH_i of ProI-arrested ovarian oocytes is low
50 (~6.7) due to the relatively high CO_2 and low O_2 concentrations in the body cavity of female
51 starfish[17]. Soon after stimulation by the hormone 1-methyladenine (1-MA)[24], pH_i increases to ~6.9[17],
52 after which the oocytes undergo GVBD and ultimately arrest at MI[16,17]. To maintain the MI arrest,
53 pH_i is maintained at ~6.9 until spawning[16,17,25-28]. The increase in pH_i following 1-MA stimulus is
54 known to require starfish NHE3 (sfNHE3)[16,17,25]. However, the upstream signaling and function of
55 this pH_i increase remain elusive.

56 For analysis of pH_i regulation, unstimulated starfish oocytes are isolated from ovaries,
57 placed in artificial seawater (ASW), and used for experiments because various techniques, such as

58 microinjection, are easily applicable to the isolated oocytes. ASW contains relatively low CO_2 and
59 high O_2 relative to the inner body cavity[17]. Due to this difference in gas concentrations, the basal pH_i
60 of isolated oocytes is ~7.0, ~0.3 units higher than that in ovarian oocytes[17]. Soon after 1-MA
61 treatment, this value increases further, to ~7.3, in a sfNHE3-dependent manner[16,17,25]. 1-MA induces
62 Gβγ-dependent activation of phosphoinositide 3-kinase (PI3K)[29-33]. Previously, we demonstrated that
63 the pHi increase is mediated by Gβγ and PI3K[16], although the molecular link between PI3K and the
64 sfNHE3-dependent pH_i increase remains unclear.

65 One candidate for this link is SGK, which is activated downstream of PI3K and
66 upregulates NHE3 in mammalian cells[6,34-36]. Mammalian SGK, which belongs to the AGC kinase
67 family[37], has three isoforms: SGK1, 2, and 3[35,38,39]. All three proteins have an activation-loop
68 (A-loop) and a C-terminal hydrophobic motif (HM)[35], but only SGK3 has the phospholipid-binding
69 domain called the Phox homology domain (PX domain)[39]. Upon agonist stimulation, the HM is first
70 phosphorylated by mammalian target of rapamycin complex 2 (mTORC2) in a PI3K-dependent
71 manner[38-40]. Phosphoinositide-dependent kinase 1 (PDK1) interacts with the phosphorylated HM and
72 phosphorylates the A-loop[41], resulting in full activation of SGK[35,36,42,43]. Although it is not known
73 whether SGK is activated in starfish oocytes, we previously showed that the C-terminus of sfNHE3
74 has a putative consensus sequence for phosphorylation by SGK, and can be phosphorylated by
75 recombinant human SGK1 *in vitro*[25]. Furthermore, PDK1 and TORC2 are functional in starfish
76 oocytes, in which they activate another AGC family kinase, Akt[37], through phosphorylation of its
77 A-loop and the HM[44,45]. In this context, Akt participates in inhibition of Myt1 and activation of
78 Cdc25[32,45-47], leading to cyclin B–Cdk1 activation through dephosphorylation of Cdk1 at Thr14 and
79 Tyr15[23,47]. Collectively, these observations inspired us to investigate whether SGK serves as a
80 downstream mediator of PI3K for the pH_i increase in starfish oocytes.

81 Another issue that remains to be resolved is the role of the pH_i increase following 1-MA
82 stimulation. Previously, we established a method for clamping pH_i at a desired value in starfish

83 oocytes[17], enabling us to examine the effects of altered pH_i. In this study, to elucidate the regulation
84 and function of the pH_i increase in oocytes, we examined the involvement of SGK in the pH_i
85 increase following 1-MA stimulus and the effects of pH_i alteration on meiotic resumption. We found
86 that SGK activation is prerequisite for two mutually independent events: pH_i increase and cyclin
87 B-Cdk1 activation. Moreover, by clamping pH_i at various values, we showed that oocytes exhibit
88 defective GVBD at reduced pH_i values. Based on these findings, we propose a model for
89 SGK-dependent meiotic resumption in starfish ovarian oocytes.

90 **Results**

91 **Starfish SGK is a homolog of human SGK3**

92 To investigate the possible involvement of SGK in the pH_i increase of oocytes during hormonal
93 stimulation with 1-MA in the starfish *A. pectinifera*, we cloned the cDNA of starfish SGK (sfSGK).
94 The open reading frame (ORF) of the cDNA encodes a polypeptide of 489 amino acids with a
95 predicted molecular mass of 56 kDa. At the amino acid sequence level, sfSGK is 52% identical to the
96 human SGK3 PX domain (Fig. 1a, blue open box) and 77% identical to the human SGK3 catalytic
97 domain (Fig. 1a, orange open box). Two phosphorylation sites, which are required for activation of
98 mammalian SGK, are conserved in sfSGK: Thr312 in the A-loop (corresponding to human SGK3
99 Thr320 which is phosphorylated by PDK1), and Thr479 in the HM (human SGK3 Ser486 which is
100 phosphorylated by mTORC2) (Fig. 1a). The transcriptome database contains no other SGK isoforms
101 for *A. pectinifera*, suggesting that SGK3 is the only member of this protein family in starfish.

102 For this study, we generated two types of antibodies: one against a recombinant fragment
103 of sfSGK lacking the N-terminal 50 amino acids (anti-sfSGK-ΔN50), and the other against a
104 C-terminal peptide (17 amino acids) containing the HM of sfSGK (anti-sfSGK-HM). We evaluated
105 the reactivity of these antibodies by immunoblotting starfish oocytes. Both antibodies detected a
106 protein of 56 kDa, corresponding the predicted molecular mass of sfSGK in unstimulated oocytes
107 (Fig. 1b, *left* and *middle* panels), suggesting that these antibodies recognized a sfSGK protein. The
108 sfSGK band underwent a mobility shift after 1-MA treatment (Fig. 1b, *left* and *middle* panels),
109 suggesting that the protein is phosphorylated after 1-MA stimulation.

110 Full activation of mammalian SGK is achieved by PDK1-dependent phosphorylation of
111 A-loop[35,41]. The amino acid sequence of the A-loop in mammalian SGK is quite similar to that of
112 sfSGK (Fig. 1a). Hence, to determine whether sfSGK is phosphorylated in the A-loop in stimulated
113 starfish oocytes, we used a commercial polyclonal anti-human phospho-SGK antibody that
114 recognizes a phosphorylated amino acid in the A-loop of mammalian SGK. The antibody detected a

115 ~59 kDa protein in stimulated oocytes, but not in unstimulated oocytes (Fig. 1b, *right* panel). In
116 addition, this band ran at the same position as the shifted bands recognized by the anti-sfSGK-ΔN50
117 and anti-sfSGK-HM antibodies (Fig. 1b). To confirm that the protein detected by the anti-human
118 phospho-SGK antibody was sfSGK, we immunoprecipitated sfSGK using the anti-sfSGK-HM
119 antibody and immunoblotted with the anti-human phospho-SGK antibody. As expected, we detected
120 protein in the bead fraction (Fig.1 c, *upper* panel, lane 8) but not the flow-through fraction (Fig.1 c,
121 *upper* panel, lane 5), indicating that the anti-human phospho-SGK antibody reacted with sfSGK.
122 Accordingly, hereafter we refer to the A-loop phosphorylation of sfSGK detected by this antibody as
123 "sfSGK-pT312 (A-loop)" in figures. Taken together, these results suggest that sfSGK is
124 phosphorylated at its A-loop, and thereby activated, in oocytes stimulated with 1-MA.
125
126 **sfSGK is activated soon after 1-MA stimulus**
127 To compare the phosphorylation dynamics of sfSGK with Akt, Cdc25 and Cdk1, we treated isolated
128 oocytes with 1-MA and analyzed them by immunoblotting. Mobility shift (Fig. 2a, sfSGK) and
129 A-loop phosphorylation (Fig. 2a, sfSGK-pT312 [A-loop]) of sfSGK was detected 1 min after 1-MA
130 stimulus. The timing of phosphorylation of Akt at Ser477 in HM by TORC2 (ref. [45]) was similar to
131 that of sfSGK (Fig. 2a, Akt-pS477 [HM]). The phosphorylation level of sfSGK increased rapidly,
132 with a peak at 3 min after 1-MA treatment (Fig. 2a, sfSGK-pT312 [A-loop]), followed by a gradual
133 decrease. A band shift of Cdc25 corresponding to hyperphosphorylation[32,47] was detected after 7 min
134 (Fig. 2a, Cdc25). Subsequently, activation of Cdk1 was detectable as dephosphorylation of Tyr15 (ref.
135 [47]) at 10 min (Fig. 2a, Cdk1-pY15), followed by onset of GVBD at approximately 17 min. These
136 results indicate that sfSGK was rapidly activated at the same time as Akt, earlier than Cdc25
137 hyperphosphorylation and cyclin B–Cdk1 activation.
138 Next, we investigated the dynamics of phosphorylation of these proteins in ovarian
139 oocytes in the body cavity, where MI arrest occurs after GVBD[16,17,27]. To this end, we injected 1-MA

140 into the body cavities of female starfish, and then at each time point, isolated two pieces of ovary:
141 one for counting GVBD, and the other for immunoblotting analysis. We found that 95% of ovarian
142 oocytes underwent GVBD within 25 min after 1-MA injection; spawning from the female started at
143 30 min. To prepare ovarian oocytes for immunoblotting, the piece of ovary was placed directly into
144 sample buffer immediately after isolation. Although these samples contained not only oocytes but
145 also other somatic cells derived from ovarian germinal epithelium, we ignored the involvement of
146 the germinal epithelium because the sfSGK, Cdc25 and Cdk1 proteins were not detectable in the
147 germinal epithelium (Fig, 2b). Analysis of oocyte-derived sfSGK, Cdc25, and Cdk1 proteins
148 revealed that both sfSGK and Cdc25 in ovarian oocytes were phosphorylated within 5 min, and that
149 Tyr15 of Cdk1 was dephosphorylated within 25 min (Fig. 2c). These results indicate that sfSGK,
150 Cdc25, and cyclin B–Cdk1 in ovarian oocytes in the body cavity were activated similarly to those in
151 isolated oocytes.
152 It should be noted that the shifted bands of sfSGK (Fig. 2a, sfSGK, lane 11-13; Fig. 2c,
153 sfSGK, lane 4) were maintained even after disappearance of the sfSGK bands reflecting
154 phosphorylation at the A-loop (Fig. 2a, sfSGK-pT312 [A-loop], lanes 11–13; Fig. 2c, sfSGK-pT312
155 [A-loop], lane 4), suggesting the existence of a phosphorylation site outside the A-loop. Given that
156 the phosphorylation site in the HM by TORC2 is conserved in sfSGK, the mobility shift may be due
157 to phosphorylation of the HM.
158
159 **PDK1 and TORC2 phosphorylate sfSGK in a PI3K-dependent manner**
160 Next, we investigated the possible involvement of PDK1 and TORC2 in the activation of sfSGK in
161 starfish oocytes. When we treated oocytes with BX795, a specific inhibitor of PDK1, A-loop
162 phosphorylation of sfSGK after 1-MA treatment was completely blocked (Fig. 2d, lane 10),
163 suggesting that PDK1 is required for A-loop phosphorylation. In mammalian cells, PDK1-dependent
164 phosphorylation of the A-loop requires prior phosphorylation of the HM by mTORC2[36,38,39,41-43]. If

165 this regulation is conserved in starfish, both the A-loop phosphorylation and HM phosphorylation of
166 sfSGK should depend on TORC2. As expected, A-loop phosphorylation was blocked by pp242, a
167 specific inhibitor of TOR, the catalytic subunit of TORC2 (Fig. 2d, lane 6). Notably, the mobility
168 shift of sfSGK was reduced by pp242, but was not affected by BX795 (Fig. 2d, lanes 6 and 10),
169 suggesting that the shift is caused by HM phosphorylation, which is dependent on TORC2 but not
170 PDK1.

171 It should be noted, however, that TOR forms two types of complex: TOR complex 1
172 (TORC1) and TORC2[48], both of which are inhibited by pp242. To confirm that the inhibition of
173 sfSGK phosphorylation by pp242 was due to inhibition of TORC2 rather than TORC1, we used the
174 TORC1 inhibitor rapamycin at a concentration previously shown to be sufficient for inhibition of
175 TORC1 in starfish oocytes[45]. Because neither A-loop phosphorylation nor the mobility shift of
176 sfSGK by 1-MA stimulation was blocked under this condition (Fig. 2d, lane 8), we concluded that
177 TORC2, but not TORC1, phosphorylates sfSGK. Taken together, these observations suggest that
178 sfSGK in starfish oocytes is activated via phosphorylation of the A-loop by PDK1 and of the HM by
179 TORC2, and that the latter is prerequisite for the former. In mammalian cells, PDK1 and TORC2
180 phosphorylate SGK3 downstream of PI3K[35,36,39,43]. Consistent with this, the pan-PI3K inhibitor
181 wortmannin blocked both A-loop phosphorylation and the mobility shift of sfSGK in starfish oocytes
182 (Fig. 2d, lane 4), suggesting that this cascade is conserved in the 1-MA-signaling pathway.

183 To separate fully-activated sfSGK from sfSGK phosphorylated only on the HM, we
184 performed Phos-tag SDS-PAGE, in which phosphorylated proteins migrate more slowly than in
185 normal SDS-PAGE[49]. sfSGK migrated as a single band in unstimulated oocytes (Fig. 2e, the *bottom*
186 band, lane 1). Two additional slower-migrating bands were detected after 1-MA stimulation (Fig. 2e,
187 the *top* and *middle* bands, lane 2). Phosphorylation of the A-loop was detected only in the top band
188 (Fig. 2e, the *top* band, lane 3), suggesting that this band corresponded to fully-activated sfSGK
189 phosphorylated by both PDK1 and TORC2. Indeed, the top band was eliminated by the PDK1

190 inhibitor BX795 and the TORC1/2 inhibitor pp242 (Fig. 2f, the *top* band, lane 5 and 6), but was
191 unchanged by the TORC1 inhibitor rapamycin. In addition, we found that the intensity of the middle
192 band was reduced by pp242, but not by BX795 or rapamycin (Fig. 2f, *middle* band, lanes 5–7),
193 suggesting that it represented sfSGK phosphorylated only on the HM by TORC2. Wortmannin
194 abolished both the top and middle bands (Fig. 2f, lane 4) indicating that all phosphorylation detected
195 using Phos-tag occurred downstream of PI3K. Taken together, these observations suggest that after
196 1-MA stimulus, PDK1 phosphorylates the A-loop of a subset of sfSGK that is pre-phosphorylated on
197 the HM by TORC2 in a PI3K-dependent manner.
198
199 **Activation of sfSGK is required for rapid pH_i increase after 1-MA stimulus**
200 Next, we investigated whether sfSGK is involved in the pH_i increase after 1-MA stimulus. Given that
201 the anti-sfSGK-HM antibody immunoprecipitated sfSGK protein (Fig. 1c), the binding of the
202 antibody to the HM may be strong enough to prevent the interaction of TORC2 with the HM of
203 sfSGK and thereby block phosphorylation of the HM. Indeed, the mobility shift of sfSGK after
204 1-MA stimulus was blocked in oocytes injected with the antibody (Fig. 3a). More importantly,
205 phosphorylation of the A-loop was also blocked (Fig. 3a), as observed in oocytes treated with pp242
206 (Fig. 2d), indicating that the anti-sfSGK-HM antibody inhibited sfSGK activation. This inhibition
207 was specific to sfSGK, because the HM of Akt was phosphorylated even in oocytes pre-injected with
208 the anti-sfSGK-HM antibody (Fig. 3a); accordingly, hereafter we refer to this antibody as an
209 sfSGK-neutralizing antibody. To determine whether sfSGK activation is required for the pH_i increase
210 after 1-MA treatment, we injected a pH-sensitive fluorescent dye, BCECF-dextran, into unstimulated
211 oocytes along with the sfSGK-neutralizing antibody, and monitored the dynamics of pH_i by
212 measuring fluorescence every 30 seconds before and after 1-MA addition. The sfSGK-neutralizing
213 antibody blocked the pH_i increase, whereas the pH_i of oocytes injected with control IgG increased
214 soon after 1-MA treatment (Fig. 3b). These results indicate that the pH_i increase after 1-MA

215 treatment depends on activation of sfSGK.

216

217 **Activation of sfSGK, but not pH_i increase, is required for cyclin B-Cdk1 activation**

218 Previously, we showed that GVBD is initiated by 1-MA in isolated oocytes even when the pH_i
219 increase is blocked[16]. Nonetheless, to our surprise, GVBD was blocked by injection of the
220 sfSGK-neutralizing antibody, whereas control IgG had no inhibitory effects on GVBD (Fig. 4a, b).
221 When we checked the phosphorylation status of Cdc25 and Cdk1 of the oocytes injected with the
222 sfSGK-neutralizing antibody, we found that neither hyperphosphorylation of Cdc25 nor
223 dephosphorylation of Tyr15 of Cdk1 after 1-MA stimulus occurred (Fig, 4c), indicating that this
224 antibody blocked 1-MA–dependent signal transduction leading to cyclin B–Cdk1 activation.

225 To verify that the inhibitory effects of the antibody were caused by specific inhibition of
226 sfSGK activation, we next performed a rescue experiment. Specifically, we replaced Thr479 of
227 sfSGK with Glu (T479E), which was expected to mimic the negatively charged phosphate group,
228 thereby causing PDK1-dependent A-loop phosphorylation even in the presence of the neutralizing
229 antibody. We co-injected mRNA encoding the mutant sfSGK-T479E and the sfSGK-neutralizing
230 antibody into unstimulated oocytes. After a 17-h incubation, the mutant was expressed and partially
231 phosphorylated on its A-loop even in the absence of 1-MA (Fig. 4d). This partial activation did not
232 induce GVBD. 1-MA stimulation induced enhancement of A-loop phosphorylation on the mutant
233 sfSGK (Fig. 4d), as well as GVBD (Fig. 4e), whereas the A-loop phosphorylation and mobility shift
234 of endogenous sfSGK were blocked in these oocytes (Fig. 4d). On the basis of these findings, we
235 concluded that the antibody-injected oocytes are rescued by the additional expression of the mutant
236 sfSGK-T479E, and that the inhibitory effect of the antibody is highly specific.

237 Interestingly, oocytes expressing the T479E mutant underwent GVBD several minutes
238 faster than the control intact oocytes (Fig. 4e), suggesting that partial activation of the mutant in
239 unstimulated oocytes likely shortened the time to GVBD following 1-MA treatment, further

240 supporting the idea that sfSGK participates in 1-MA signaling leading to GVBD. We also found that
241 the band of the T479E mutant phosphorylated on the A-loop underwent an upward mobility shift
242 after 1-MA stimulation, indicating that the mutant was phosphorylated on a site outside the A-loop
243 and the HM; however, the function of this phosphorylation event remains unclear. Taken together,
244 these results suggest that activation of sfSGK is required for cyclin B–Cdk1 activation.
245 Although the 1-MA–induced pH_i increase and cyclin B–Cdk1 activation were
246 simultaneously blocked by the sfSGK-neutralizing antibody, they were independent of each other.
247 We base this claim on two lines of evidence: 1) The increase in pH_i occurred earlier than cyclin B–
248 Cdk1 activation (Fig. 2a, 3b), and was not affected by treatment with the Cdk1 inhibitor, roscovitine
249 (Supplementary Fig. 1), indicating that the pH_i increase is independent of cyclin B–Cdk1 activation.
250 2) GVBD in isolated oocytes, in which initial pH_i before 1-MA stimulation is ~7.0, is initiated even
251 when the pH_i increase was blocked by an NHE inhibitor or by treatment with sodium-free ASW[16],
252 indicating that the cyclin B–Cdk1 activation leading to GVBD is independent of the pH_i increase
253 (see also below, Fig. 5a). Thus, the pH_i increase and cyclin B–Cdk1 activation are mutually
254 independent events.
255
256 **Reduced pH_i delays onset of GVBD and blocks completion of GVBD without affecting cyclin**
257 **B–Cdk1 activation**
258 To elucidate the role of the pH_i increase, we investigated effect of altered pH_i on 1-MA–induced
259 meiotic resumption in starfish oocytes. To clamp pH_i, oocytes were incubated in sodium-free ASW
260 containing CH_3COONH_4 (modified ASW), in which the pH_i was adjusted to the desired value with
261 CH_3COONH_4 but did not increase after 1-MA stimulation because of the absence of sodium ion[17]
262 (see also Materials & Methods). We clamped pH_i at 6.7, corresponding to the value in unstimulated
263 ovarian oocytes[17]; as well as 7.0 and 7.2, similar to the values in isolated oocytes before and after
264 1-MA stimulus, respectively[17]. First, we examined effects of pH_i clamping on sfSGK and cyclin B–

265 Cdk1 activation after 1-MA stimulus. Immunoblotting analysis showed that the phosphorylation
266 status of sfSGK, Cdc25, and Cdk1 in oocytes at all clamped pH_i values was basically same as in
267 oocytes in ASW (Fig. 5a). This observation suggests that 1-MA–induced signaling leading to cyclin
268 B–Cdk1 activation does not depend on pH_i, and further supports our conclusion that the pH_i increase
269 is not required for cyclin B–Cdk1 activation.

270 After cyclin B–Cdk1 activation, the onset of GVBD was delayed for several minutes at a
271 clamped pHi of 6.7 (Fig. 5b), as previously reported[17]. At clamped pH_i values of 7.0 and 7.2, the
272 times of GVBD onset were similar to those in ASW (Fig. 5b). At all clamped pH_i values, the
273 morphology of GVBD onset was indistinguishable from those in ASW: before 1-MA stimulation, the
274 rim of GV looked like a clear line under the microscope; at GVBD onset, cytoplasmic granules
275 started to invade from the rim into the inner GV area (Supplementary Fig. 2). These results suggest
276 that after cyclin B–Cdk1 activation, time to onset of GVBD is weakly pH_i-dependent.

277 More importantly, we observed a remarkable defect after onset of GVBD. In ASW,
278 cytoplasmic granules occupied the whole inner GV area within 15 min after GVBD onset, indicating
279 completion of GVBD (Fig. 5c, Supplementary Movie 1, Supplementary Fig. 3). At a clamped pH_i of
280 6.7, however, we found that the invasion of granules proceeded slowly and stalled around 40 min,
281 remaining incomplete even 60 min after GVBD onset (Fig. 5c, Supplementary Movie 2,
282 Supplementary Fig. 3). At a clamped pH_i of 7.0, invasion proceeded further and finished with a trace
283 of inner GV area within 40–50 min (Fig. 5c, Supplementary Movie 3, Supplementary Fig. 3). At
284 clamped pH_i of 7.2, the granules invaded and ultimately distributed homogenously throughout the
285 oocytes within 20–30 min after GVBD onset (Fig. 5c, Supplementary Movie 4, Supplementary Fig.
286 3). These observations suggest that progression of granule invasion is sensitive to pH_i; in particular,
287 completion of GVBD is drastically impaired at a pH_i of 6.7. Given that the pH_i of unstimulated
288 ovarian oocytes is around 6.7 (ref. [17]), the pH_i increase mediated by sfSGK is likely required for
289 completion of GVBD in ovarian oocytes.

290 **Discussion**

291 The results of this study show that sfSGK is activated by TORC2 and PDK1 in a PI3K-dependent
292 manner after 1-MA stimulus in starfish oocytes. We found that sfSGK is required for regulation of
293 two mutually independent pathways leading to pH_i increase and cyclin B–Cdk1 activation.
294 Furthermore, we identified the presence of a pH_i-sensitive process in meiotic resumption: although
295 1-MA signaling leading to cyclin B–Cdk1 activation is pH_i-independent, the subsequent onset time
296 and completion of GVBD are pH_i-dependent.

297 On the basis of previous studies and the present findings, we propose a model for meiotic
298 resumption in ovarian oocytes (Fig. 6). In this model, sfSGK exerts two essential functions: cyclin
299 B–Cdk1 activation, which induces meiotic resumption, and pH_i increase, which promotes completion
300 of GVBD (Fig. 6). In living starfish, ovarian oocytes reside in coelomic fluid in the body cavity.
301 Previously, we reported that the coelomic fluid has relatively high CO_2 and low O_2 concentrations
302 relative to ASW[17]. Under these gas conditions, the pH_i of unstimulated ovarian oocytes is around 6.7,
303 and increases after 1-MA stimulation[17]. As shown in Fig. 2c, sfSGK is activated in ovarian oocytes
304 after 1-MA stimulus in the body cavity. Subsequently, sfSGK likely induces the pH_i increase and
305 cyclin B–Cdk1 activation in ovarian oocytes (Fig. 6), as demonstrated in isolated oocytes (Figs. 3
306 and 4). Thereafter, cyclin B–Cdk1 causes GVBD. However, if pH_i in ovarian oocytes was not
307 increased from 6.7 soon after 1-MA stimulus, GVBD would initiate after a delay and fail to complete,
308 as we observed when pH_i was clamped at 6.7 in isolated oocytes (Fig. 5). Thus, in ovarian oocytes,
309 the sfSGK-dependent pH_i increase would determine the time of GVBD onset after cyclin B–Cdk1
310 activation and be a prerequisite for completion of GVBD (Fig. 6).

311 In the ovaries, starfish oocytes arrest at MI after GVBD [16,17,27]. This arrest is released upon
312 spawning, at which time the oocytes are ready to be fertilized[16,17,27]. Fertilization during the period
313 between release from the MI arrest and the first polar body formation is important for monospermy,
314 because insemination before GVBD or after polar body formation tends to result in polyspermy[27,50].

315 Thus, the sfSGK-dependent pH_i increase soon after 1-MA may ensure that ovarian oocytes proceed
316 to MI arrest before spawning, helping to promote monospermy. In addition, to ensure fertilization
317 before polar body formation, MI arrest must be maintained until spawning[27]. To maintain MI arrest,
318 sfSGK-dependent pH_i increase should not exceed 7.0, because release from MI arrest occurs at
319 pH_i>7.0 (ref. [16,17,26,27]). In this study, A-loop phosphorylation of sfSGK became undetectable around
320 the time of the end of pH_i increase (Fig. 2a, c). Therefore, sfSGK inactivation may be important to
321 stop the pH_i increase for maintaining MI arrest. Interestingly, the A-loop was dephosphorylated even
322 in the presence of phosphorylated HM (Fig. 2a, c), implying the presence of regulatory mechanism
323 of A-loop dephosphorylation that is not associated with dephosphorylation of the HM, such as
324 up-regulation of an A-loop phosphatase. To our knowledge, regulation of SGK inactivation has never
325 been investigated in any animal, and this issue should be examined in a future study.

326 Although mammalian SGKs are involved in cell proliferation[51,52], their function in
327 M-phase remains unclear. Here, we showed that sfSGK is required for cyclin B–Cdk1 activation in
328 starfish oocytes (Fig. 4). In parallel with the present study, Hiraoka et al. demonstrated that sfSGK
329 directly phosphorylates Cdc25 and Myt1 to activate cyclin B–Cdk1, and that sfSGK, rather than Akt,
330 is the major kinase responsible for induction of cyclin B–Cdk1 activation[53]. These are the first
331 reports to demonstrate the involvement of SGK in cyclin B–Cdk1 activation.

332 In addition, we showed that sfSGK is required for the pH_i increase (Fig. 3b). Previously,
333 we reported that this increase depends on sfNHE3[16,17,25]. In human cultured cells, NHE-dependent
334 pH_i increase is upregulated by phosphorylation of C-terminal region of NHE that leads to NHE
335 activation[7,9], and/or by accumulation of NHE protein on the plasma membrane through trafficking of
336 endosomal NHE to the plasma membrane[6]. Although it is not known whether these mechanisms are
337 functional in starfish oocytes, it is clear from our previous work that the C-terminus of sfNHE3 is
338 phosphorylated by human SGK1 *in vitro*[25]. Therefore, we speculate that sfSGK upregulates sfNHE3
339 by direct phosphorylation of its C-terminus.

340 In the process of GVBD in starfish oocytes, the nuclear pore complex on nuclear envelopes
341 (NEs) of the GV are first disassembled[54-56], and then the NEs are rapidly broken into membrane
342 fragments, followed by complete mixing of cytoplasm and nucleoplasm[54,55]. GVBD onset, as judged
343 by differential interference contrast (DIC) microscopy in this study, likely represents the time of
344 membrane fragmentation, as a clear boundary between cytoplasm and GV was still observed by DIC
345 during nuclear pore disassembly[55]. One possible interpretation of the remarkable blockage of GVBD
346 completion at a clamped pH_i of 6.7 (Fig. 5b, c) is that incomplete NE fragmentation occurred and
347 disrupted invasion of cytoplasmic granules. Given that NE fragmentation depends on F-actin shell
348 formed on the inner surface of the GV[56], our present observations imply that the formation or
349 function of this shell is blocked at pH_i 6.7. Although this possibility is yet to be tested, F-actin
350 architecture is known to be disrupted by lower pH_i, at least in mouse mammary tissue[57].
351 pH_i increase after release from ProI arrest has also been reported in frog[13], urodele[58], and
352 surf clam[12]. In *Xenopus* oocytes, NHE-dependent pH_i increase after hormonal stimulation[13,14,59] has
353 been suggested to accelerate cyclin B–Cdk1 activation by promoting accumulation of Mos protein,
354 which participates in cyclin B–Cdk1 activation[60]. By contrast, we found that cyclin B–Cdk1
355 activation was independent of the pH_i increase. One potential reason for this difference could be
356 cyclin B–Cdk1 activation in starfish oocytes does not require synthesis of new protein[61], including
357 Mos[62]. In addition, pH_i increase in *Xenopus* oocytes plays a role in migration of GV to the animal
358 pole before GVBD[63]. Such migration does not occur in starfish oocytes because the GV already
359 resides at the animal pole even in ProI-arrested oocytes. Instead, we found that completion of GVBD
360 depends on pHi. Thus, starfish and *Xenopus* oocytes provide suitable models for understanding
361 different aspects of pH_i-dependent regulation of the meiotic cell cycles.
362 In summary, we showed that sfSGK is required for pH_i increase and cyclin B–Cdk1
363 activation in starfish oocytes, and that completion of GVBD is a pH_i-sensitive process. These
364 findings reveal a novel role for SGK in control of meiotic cell cycles and emphasize the importance

365 of tight regulation of pH_i in oocyte meiosis.

366 **Materials and methods**

367 **Oocyte preparation.** Starfish (*Asterina pectinifera*) were collected on Pacific coast of Japan, and
368 kept in laboratory aquaria supplied with circulating seawater at 14°C. Fully-grown ProI-arrested
369 oocytes were isolated from ovaries and treated with calcium-free artificial seawater (calcium-free
370 ASW: 476 mM NaCl, 10 mM KCl, 36 mM $MgCl_2$, 18 mM $MgSO_4$, 20 mM H_3BO_3, pH 8.2) to
371 remove follicle cells. Subsequently, the oocytes were kept in artificial seawater (ASW: 462 mM
372 NaCl, 10 mM $CaCl_2$, 10 mM KCl, 36 mM $MgCl_2$, 18 mM $MgSO_4$, 20 mM H_3BO_3, pH 8.2) until use.
373 For 1-MA stimulation, the isolated oocytes were incubated with ASW containing 0.5 μM 1-MA at
374 23°C, and then collected for analysis. To induce meiotic resumption of ovarian oocytes in the body
375 cavity, 1 ml of calcium-free ASW without boric acid (462 mM NaCl, 10 mM KCl, 36 mM $MgCl_2$, 17
376 mM $MgSO_4$) containing 0.5 mM 1-MA was injected into the body cavity of female starfish. Pieces of
377 ovary containing stimulated oocytes were directly recovered from the body cavity, and then
378 immediately added into a sample buffer (0.25 M Tris-HCL [pH 6.8], 40% glycerol, 8% SDS, 20%
379 2-mercaptoethanol, 0.01% bromophenol blue). To compare proteins in germinal epithelium with
380 those in oocytes, a piece of ovary was isolated from the body cavity and separated into germinal
381 epithelium and oocytes. These fractions were separately recovered into different tubes, each of which
382 contained an equal volume of sample buffer, boiled at 95°C for 5 min, and subjected to
383 immunoblotting analysis.

384

385 **cDNA cloning of starfish SGK.** To isolate a cDNA encoding the starfish homolog of SGK, total
386 mRNA was isolated from ProI-arrested ovarian oocytes using RNAwiz (Ambion, Thermo Fisher
387 Scientific; Waltham, MA, USA). The first-strand cDNA library was prepared from total mRNA using
388 the TAKARA RNA PCR Kit (AMV) Ver.2.1 and Prime Script Reverse Transcriptase (Takara Bio;
389 Shiga, JP) with random 9-mers. A 250-bp cDNA fragment (fragment 1) was first obtained by
390 reverse-transcriptase (RT)-PCR with degenerate primers designed based on amino acid sequences

391 conserved among human, mouse, sea urchin, and *C. elegans* SGKs (forward: YAVKVL,
392 5'-TAYGCNGTNAARGTNYT-3', and reverse: FYAAEIA, 5'-AARATRCGNCGNCTYTCDCG-3').
393 Because 3' and 5' rapid amplification of cDNA ends (RACE) with specific primers designed against
394 fragment 1 were unsuccessful, we obtained another fragment (fragment 2) that partially overlapped
395 with fragment 1, as follows: a forward specific primer (5'-CCCGACAAGCTCTAC-3') was
396 designed against fragment 1, and a reverse degenerate primer (GLPPFY,
397 5'-CCNRANGGNGGNAARAT-3') was designed against a conserved amino acid sequence in the
398 SGK alignment that is located in a region approximately 85 amino acids C-terminal to the region of
399 the first reverse degenerate primer. The 360-bp fragment 2 was obtained by RT-PCR using these
400 primers. Next, to identify the 3' end, another first-strand cDNA library was generated from the total
401 mRNA using RNA PCR Kit (AMV) Ver. 2.1 and Prime Script Reverse Transcriptase (Both, Takara
402 Bio; Shiga, JP) using the oligo dT-Adaptor primer from the kit. Then, RT-PCR was performed on the
403 cDNA library using a specific forward primer designed against the 5' region of fragment 2
404 (5'-CCCCAGAAGTCTTGAAGAA-3') and the adaptor primer (5'-GTTTTCCCAGTCACGAC-3').
405 Using the RT-PCR product as a template, nested PCR was performed with another forward specific
406 primer (5'-GGAGTATGATCGTAGTGTAG-3') and the adaptor primer, resulting in amplification of
407 a ~600 bp 3' RACE product. Next, the 5' ends were identified by RACE using 5'-Full RACE Core
408 Set (Takara Bio; Shiga, JP) with specific primers (reverse for generating first-strand cDNA:
409 5'-CCAAAGTCTGTCAAC-3'; forward for first PCR: 5'-CAGAGATTTGAAGCCGGAG-3',
410 reverse for first PCR: 5'-GTTCAGGGAAGCATCTCTTCT-3'; forward for nested PCR:
411 5'-GCCGGAGAACATTTTGATTG-3', reverse for nested PCR:
412 5'CTCTCTCTGCAGATGGAAGA-3'), resulting in amplification of a 1.5-kb 5' RACE product. The
413 full-length ORF was PCR-amplified from the cDNA library generated using random 9mers with
414 pfx50 DNA polymerase (Thermo Fisher Scientific) and specific primers (forward:
415 5'-GGGGCCCCTGGGATCCATGGCTGCCAACAGTACTAG-3'; reverse:

416 5'-GTCGACCCGGGAATTCTTAGTCGTCAAATGCCTCG-3'). The amplified cDNA was inserted
417 into vector pGEX-6P-3 (GE Healthcare; Little Chalfont, UK) using the In-Fusion HD Cloning Kit
418 (Takara Bio; Shiga, JP) and sequenced.
419
420 **Immunoprecipitation.** For preparation of oocyte extracts, oocytes were recovered in ASW before
421 and after 1-MA treatment. After freezing in liquid N_2, lysis buffer [80 mM β-glycerophosphate, 20
422 mM EGTA, 10 mM Mops pH 7.0, 100 mM sucrose, 100 mM KCl, 1 mM DTT, 0.5 % NP-40, 1%
423 protease inhibitor cocktail (Nacalai Tesque; Kyoto, JP), and 1% phosphatase inhibitor cocktails 1 and
424 2 (Sigma; St Louis, MO, USA)] was added to the oocytes, followed by vortexing and centrifugation
425 at 12,500× *g* for 15 min. The supernatant was used as the extract. For immunoprecipitation, 15 μl of
426 oocyte extract (1 oocyte per 1 μl) was added to 3 μl of protein A–Sepharose 4B (Sigma) to which 7.0
427 μg of anti-sfSGK-HM antibody or control IgG had been pre-adsorbed and cross-linked using borate
428 buffer containing 25 mM DSS (25 mM DSS, 0.2 M H_3BO_3 [pH 9.0], 0.2 M NaOH), followed by
429 incubation for 90 min on ice. Beads and flow-through were separated, and sample buffer was added.
430 The samples were boiled at 95°C for 5 min and subjected to immunoblotting analysis.
431
432 **Chemicals.** Wortmannin (LC laboratories; Woburn, MA, USA), pp242 (Cayman Chemical; Ann
433 Arbor, MI, USA), rapamycin (FUJIFILM Wako pure chemical; Osaka, JP), BX795 (Enzo Life
434 Sciences; New York, NY, USA), and roscovitine (Merck, Darmstadt, BRD) were dissolved in DMSO
435 at 20 mM as a stock solution, and used at final concentrations of 40, 2, 20, 6, and 30 μM,
436 respectively.
437
438 **DNA construct.** A mutant sfSGK in which Thr479 was replaced with Glu was generated by PCR
439 using PrimeSTAR MAX Polymerase (Takara Bio; Shiga, JP) with primers containing the point

440 mutation (forward: 5'-GGCTTCGAATATGTCCCACCAAGCGAG-3', and reverse:
441 5'-GACATATTCGAAGCCAGTAAAGGCAGAG-3'). The mutated cDNA was inserted into the
442 pSP64-S-based vector, in which its SP6 promoter was replaced with a T7 promoter[32], with the *A.*
443 *pectinifera* cyclin B Kozak sequence (5'-TACAAT-3') and a 3× FLAG-tag at C-terminus.
444
445 **Antibodies.** The anti-sfSGK-ΔN50 rabbit polyclonal antibody was raised against a Nus- and
446 His-tagged recombinant sfSGK fragment lacking the N-terminal 50 amino acids including the PX
447 domain. The antibody was purified from the antiserum using PVDF membrane on which a
448 recombinant GST-tagged sfSGK protein had been blotted. The anti-sfSGK-HM rabbit polyclonal
449 antibody was raised against a synthetic peptide representing the 17 C-terminal amino acids
450 containing the HM (Ser473-Asp489) of sfSGK, and affinity-purified using antigen peptide–
451 conjugated Sulfo Link Coupling Resin (Thermo Fisher Scientific). The control IgG was purified
452 from rabbit pre-immune serum using protein A–Sepharose 4B (Sigma). For microinjection, the
453 anti-sfSGK-HM antibody and control IgG were further concentrated using a 50-kDa cut-off Amicon
454 Ultra (Merck; Rahway, NJ, USA), and the buffer was replaced with injection buffer (0.05% NP-40 in
455 PBS buffer, pH 7.2). Preparation of anti-starfish phospho-Akt (Ser477) rabbit polyclonal antibody[45],
456 anti-starfish Akt (sfAkt) C-terminus rabbit polyclonal antibody[46], anti-starfish Cdc25 (sfCdc25)
457 rabbit polyclonal antibody[47], and anti-PSTAIR antibody for Cdk1 (ref. [45]) were described previously.
458 The anti-phospho-Tyr15 Cdk1 antibody and anti-human phospho-SGK rabbit polyclonal antibody
459 [p-SGK (Thr 256)-R] were purchased from Cell Signaling Technology (Danvers, MA, USA) and
460 Santa Cruz Biotechnology (Dallas, TX, USA), respectively. Peroxidase-conjugated anti-rabbit IgG
461 and anti-mouse IgG, used as secondary antibodies in immunoblotting, were purchased from GE
462 healthcare (Little Chalfont, UK) and Dako (Glostrup, Denmark), respectively.
463

464 **Microinjection.** Microinjection was performed as previously described[64,65]. The anti-sfSGK-HM
465 antibody or control IgG was injected into unstimulated oocytes at 23°C at a final concentration in the
466 oocyte of 65.2 μg/ml, followed by incubation for 1 h. For expression of sfSGK (T479E), the mutant
467 was transcribed from the pSP64-S-based vector construct using the mMESSAGE mMACHINE kit
468 (Ambion, Thermo Fisher Scientific), dissolved in water, and injected into unstimulated oocytes (30
469 pg per oocyte). After further incubation for 17 h at 20°C, these oocytes were treated with 0.5 μM
470 1-MA and recovered for immunoblotting analysis at 4 min. The rest of the oocytes were observed to
471 count GVBD.
472
473 **Immunoblotting.** Oocytes (five for normal SDS-PAGE, six for Phos-tag-SDS-PAGE) were
474 recovered in 3 μl of seawater, added directly to 3 μl of 2× sample buffer, and immediately frozen in
475 liquid N_2. After thawing and boiling for 5 min at 95°C, proteins were separated on polyacrylamide
476 gels (8% for sfSGK only, 8.5% for sfSGK and Cdk1). For Phos-tag SDS-PAGE, 8% polyacrylamide
477 gel containing 60 μM Phos-tag acrylamide (FUJIFILM Wako Pure Chemical co.; Osaka, JP) and 600
478 μM $ZnCl_2$ was used. Immunoblotting was performed as previously described[32]. Antibodies used for
479 immunoblotting were as follows: anti-sfSGK-ΔN50 (1:2,000, in TBS-T), anti-sfSGK-HM (1:1000,
480 in TBS-T), anti-human phospho-SGK (1:400, in TBS-T), anti-sfAkt-pS477 (1:600, in Can Get Signal
481 Immunoreaction Enhancer Solution 1 [Can Get sol. 1], TOYOBO, Osaka, Japan),
482 anti-sfAkt-C-terminus (1:400, in Can Get sol. 1), anti-sfCdc25 (1:2000, in Can Get sol. 1), an
483 anti-Cdk1-pY15 (1:1000, in Can Get sol. 1), and anti-PSTAIR (1:50,000, in Can Get sol. 1).
484 horseradish peroxidase (HRP)-conjugated anti-rabbit IgG (1: 2000, in TBS-T or Can Get sol. 2) and
485 anti-mouse IgG (1:2000, in Can Get sol. 2) were used as secondary antibodies. Proteins reacting with
486 the antibodies were visualized with ECL prime (GE healthcare; Little Chalfont, UK), and digital
487 images were acquired on a LAS4000 mini imager (Fujifilm; Tokyo, JP).
488

489 **Measurement of pH_i with BCECF-dextran.** A dextran (10-kDa)-conjugate of
490 2',7'-bis-(2-carboxyethyl)-5(and-6)-carboxyfluorescein (BCECF) (Molecular Probes, Thermo Fisher
491 Scientific) was dissolved at a concentration of 2 mM in injection buffer (100 mM potassium
492 aspartate, 10 mM HEPES, 0.05% NP-40, pH 7.2). BCECF-dextran (20 pl per oocyte) and either the
493 sfSGK-HM antibody or control IgG (final 65.2 μg /ml in an oocyte) were co-injected into
494 unstimulated oocytes. After incubation for 1 h, the pH_i of these oocytes was measured every 30
495 seconds before and after 1-MA treatment. pH_i measurements with BCECF-dextran were made by
496 determining the pH-dependent ratio of its emission intensity (detected at 535 nm) when excited at
497 495 nm versus its isosbestic point of 436 nm. Calibration of pH_i from the intensity ratio was
498 performed as previously described[17]. All fluorescence images were captured and analyzed using a
499 NIKON ECLIPSE Ti-U fluorescent microscope (Nikon Instech; Tokyo, JP), which was connected to
500 a CMOS camera (ORCA-Flash2.8, C11440-10C; Hamamatsu Photonics; Hamamatsu, JP) controlled
501 by an HCImage processing system (Hamamatsu Photonics; Hamamatsu, JP). Excitation light from a
502 xenon lamp alternated between 436 nm and 495 nm under computational control. The emitted light
503 passed through a dichroic beam splitter at 505 nm and through a 510–560 nm emission filter.
504
505 **Clamping pH_i of oocytes.** NH_4Cl dissolved in seawater forms NH_3, which crosses cell membrane
506 easily and binds H^+, causing an increase in pH_i. By contrast, when CH_3COONa is dissolved in
507 seawater, it forms CH_3COOH, which crosses cell membrane easily and releases H^+ into the cell,
508 causing pHi to decrease. By applying this principle, Hamaguchi *et al.* found that extracellular pH
509 (pH_o) and pH_i were almost equal when sea urchin eggs were treated with ASW containing 20 mM
510 CH_3COONa and NH_4Cl[66]. We showed previously that when starfish oocytes are incubated in
511 sodium-free ASW containing CH_3COONH_4 at various pH values (modified ASW: 480 mM choline
512 chloride, 55 mM $MgCl_2$, 5 mM KCl, 10 mM PIPES, 10 mM HEPES, 20 mM CH_3COONH_4, 9.2 mM
513 $CaCl_2$), the pH_i of oocytes was invariably ~0.2 units higher than pH_o[17]. Hence, to clamp pH_i of

514 oocytes at 6.7, 7.0, and 7.2, unstimulated oocytes were incubated with modified ASW with a pH of
515 6.5, 6.8, and 7.0, respectively, for 20 min. These oocytes were then treated with 1-MA, followed by
516 observation of GVBD or immunoblotting analysis. It should be noted that because sodium ion is not
517 present in modified ASW, the sfNHE3-dependent pH_i increase mediated by Na^+/H^+ exchange does
518 not occur, so pHi is maintained at the clamped value even after 1-MA treatment. As a control,
519 isolated oocytes were incubated in ASW (pH_o 8.2), in which the pHi of unstimulated oocytes was
520 ~7.0. Because ASW contains sodium ions, a sfNHE3-dependent pH_i increase to 7.2–7.3 occurs after
521 1-MA treatment[17]; see also the control IgG–injected oocytes in Fig. 3b.

522 **Oocyte observation.** GVBD onset was visually judged by focusing the microscope on the equatorial
523 plane of the GV: the rim of intact GV appears as a sharp line in unstimulated oocytes, but becomes
524 fuzzy at GVBD onset. All DIC images and DIC image sequences were captured on a NIKON
525 ECLIPSE Ti-U microscope (Nikon Instech; Tokyo, JP), which was connected to a CMOS camera
526 (ORCA-Flash2.8, C11440-10C; Hamamatsu Photonics; Hamamatsu, JP) controlled by a HCImage
527 processing system (Hamamatsu Photonics; Hamamatsu, JP). For time-lapse recording, DIC images
528 were collected every 10 seconds. Z-stack images were captured soon after time-lapse imaging.

529 **Data availability**

530 Data supporting the findings of this study are available within the article or upon reasonable request
531 to the corresponding authors.

532

533 **Acknowledgements**

534 We thank M. Matsushita for raising the anti-starfish SGK-ΔN50 antibody, M. Terasaki for providing
535 vector pSP64-S, and E. Okumura for providing anti-sfCdc25 and anti-sfAkt C-terminus antibodies.
536 We also thank K. Yura for his contribution to perform alignment of SGK isoforms. This work was
537 supported by JSPS KAKENHI grant numbers 17K07405, Takeda Science Foundation, and the
538 Cooperative Program provided by The Atmosphere and Ocean Research Institute, The University of
539 Tokyo.

540

541 **Author contributions**

542 E.H., D.H., and K.C. conceived and designed all the experiments, and E.H. performed all the
543 experiments. Cloning of cDNA encoding sfSGK was performed by S.O. and N.H. All authors
544 discussed the results. E.H., D.H., T.K., and K.C. wrote the manuscript.

545

546 **Competing interests**

547 The authors declare no competing interests.

548

549 **Materials and correspondence**

550 Correspondence and requests for materials should be addressed to K.C.

551 **References**

552 1. Baltz, J. M. Intracellular pH regulation in the early embryo. *Bioessays* **15**, 523–530 (1993).

553 2. Schatten, G., Bestor, T., Balczon, R., Henson, J. & Schatten, H. Intracellular pH shift initiates
554 microtubule-mediated motility during sea urchin fertilization. *Ann. N. Y. Acad. Sci.* **466**, 940–944
555 (1986).

556 3. Grandin, N. & Charbonneau, M. Cycling of intracellular pH during cell division of Xenopus
557 embryos is a cytoplasmic activity depending on protein synthesis and phosphorylation. *J. Cell*
558 *Biol.* **111**, 523–532 (1990).

559 4. Grillo-Hill, B., Choi, C., Jimenez-Vidal, M. & Barber, D. Increased H^+ efflux is sufficient to
560 induce dysplasia and necessary for viability with oncogene expression. *Elife* **4**, 10.7554/eLife.03270.
561 (2015).

562 5. Orlowski, J. & Grinstein, S. Diversity of the mammalian sodium/proton exchanger SLC9 gene
563 family. *Pflugers Archi.* **447**, 549–565 (2004).

564 6. He, P. et al. Serum- and glucocorticoid-induced kinase 3 in recycling endosomes mediates acute
565 activation of Na^+/H^+ exchanger NHE3 by glucocorticoids. *Mol. Biol. Cell* **22**, 3812–3825 (2011).

566 7. Wang, D., Sun, H., Lang, F. & Yun, C. Activation of NHE3 by dexamethasone requires
567 phosphorylation of NHE3 at Ser663 by SGK1. *Am J Physiol. Cell Physiol.* **289**, C802–C810 (2005).

568 8. Yun, C. C. Concerted roles of SGK1 and the Na^+/H^+ exchanger regulatory factor 2 (NHERF2) in
569 regulation of NHE3. *Cell Physiol. Biochem.* **13**, 29–40 (2003).

570 9. Takahashi, E. et al. $p90^{RSK}$ is a serum-stimulated Na^+/H^+ exchanger isoform-1 kinase.
571 Regulatory phosphorylation of serine 703 of Na^+/H^+ exchanger isoform-1. *J. Biol.*
572 *Chem.* **274**, 20206–20214 (1999).

573 10. Wang, C. et al. Somatostatin stimulates intestinal NHE8 expression via p38 MAPK
574 pathway. *Am. J. Physiol. Cell Physiol.* **300**, C375–C382 (2011).

575 11. Xu, H., Ghishan, F. & Kiela, P. SLC9 gene family: function, expression, and regulation. *Copr.*
576 *Physiol.* **8,** 555–583 (2018).
577 12. Dubé, F. & Eckberg, W. Intracellular pH increase driven by an Na^+/H^+ exchanger upon
578 activation of surf clam oocytes. *Dev. Biol.* **190**, 41–54 (1997).
579 13. Lee, S. & Steinhardt, R. pH changes associated with meiotic maturation in oocytes of Xenopus
580 laevis. *Dev. Biol.* **85,** 358–369 (1981).
581 14. Rezai, K., Kulisz, A. & Wasserman, W. J. Protooncogene product, c-mos kinase, is involved in
582 upregulating Na^+/H^+ antiporter in Xenopus oocytes. *Am. J. Physiol.* **267**, C1717–1722 (1994).
583 15. Miyazaki SI, Ohmori H, & Sasaki S. Potassium rectifications of the starfish oocyte membrane
584 and their changes during oocyte maturation. *J. Physiol.* **246**, 55-78. (1975)
585 16. Harada, K., Oita, E. & Chiba, K. Metaphase I arrest of starfish oocytes induced via the MAP
586 kinase pathway is released by an increase of intracellular pH. *Development* **130,** 4581–4586 (2003).
587 17. Moriwaki, K., Nakagawa, T., Nakaya, F., Hirohashi, N. & Chiba, K. Arrest at metaphase of
588 meiosis I in starfish oocytes in the ovary is maintained by high CO_2 and low O_2 concentrations in
589 extracellular fluid. *Zoolog. Sci.* **31**, 975–984 (2013).
590 18. Masui, Y. From oocyte maturation to the *in vitro* cell cycle: the history of discoveries of
591 Maturation-Promoting Factor (MPF) and Cytostatic Factor (CSF). *Differentiation* **69**, 1–17 (2001).
592 19. Hunt, T. Maturation promoting factor, cyclin and the control of M-phase. *Curr. Opin. Cell*
593 *Biol.* **1**, 268–274 (1989).
594 20. Nurse, P. Universal control mechanism regulating onset of M-phase. *Nature* **344**, 503–508
595 (1990).
596 21. Kishimoto, T. Entry into mitosis: a solution to the decades-long enigma of MPF. *Chromosoma*
597 **124**, 417–428 (2015).
598 22. Chiba, K. Evolution of the acquisition of fertilization competence and polyspermy blocks
599 during meiotic maturation. *Mol. Reprod. Dev.* **78**, 808–813 (2011).

600 23. Kishimoto, T. MPF-based meiotic cell cycle control: Half a century of lessons from starfish
601 oocytes. *Proc. Jpn. Acad. Ser. B. Phys. Biol. Sci.* **94**, 180–203 (2018).
602 24. Kanatani, H., Shirai, H., Nakanishi, K. & Kurokawa, T. Isolation and indentification of meiosis
603 inducing substance in starfish *Asterias amurensis*. *Nature* **221**, 273–274 (1969).
604 25. Harada, K., Fukuda, E., Hirohashi, N. & Chiba, K. Regulation of intracellular pH by
605 p90Rsk-dependent activation of an Na^+/H^+ exchanger in starfish oocytes. *J. Biol. Chem.* **285**, 24044–
606 24054 (2010).
607 26. Oita, E., Harada, K. & Chiba, K. Degradation of polyubiquitinated Cyclin B is blocked by the
608 MAPK pathway at the Metaphase I arrest in starfish oocytes. *J. Biol. Chem.* **279**, 18633–18640
609 (2004).
610 27. Usui, K., Hirohashi, N. & Chiba, K. Involvement of mitogen-activating protein kinase and
611 intracellular pH in the duration of the metaphase I (MI) pause of starfish oocytes after spawning. *Dev.*
612 *Growth Differ.* **50**, 357–364 (2008).
613 28. Ochi, H., Aoto, S., Tachibana, K., Hara, M. & Chiba, K. Block of CDK1-dependent
614 polyadenosine elongation of Cyclin B mRNA in metaphase-I-arrested starfish oocytes is released by
615 intracellular pH elevation upon spawning. *Mol. Reprod. Dev.* **83**, 79–87 (2016).
616 29. Shilling, F., Chiba, K., Hoshi, M., Kishimoto, T. & Jaffe, L. Pertussis toxin inhibits
617 1-methyladenine-induced maturation in starfish oocytes. *Dev. Biol.* **133**, 605–608 (1989).
618 30. Chiba, K., Kontani, K., Tadenuma, H., Katada, T. & Hoshi, M. Induction of starfish oocyte
619 maturation by the βγ subunit of starfish G protein and possible existence of the subsequent effector in
620 cytoplasm. *Mol. Biol. Cell* **4**, 1027– 1034 (1993).
621 31. Sadler, K. & Ruderman, J. Components of the signaling pathway linking the 1-methyladenine
622 receptor to MPF activation and maturation in starfish oocytes. *Dev. Biol.* **197**, 25–38 (1998).

623 32. Hiraoka, D., Aono, R., Hanada, S., Okumura, E. & Kishimoto, T. Two new competing
624 pathways establish the threshold for cyclin-B–Cdk1 activation at the meiotic G2/M transition. *J. Cell*
625 *Sci.* **129**, 3153–3166 (2016).
626 33. Vanhaesebroeck, B., Guillermet-Guibert, J., Graupera, M. & Bilanges, B. The emerging
627 mechanisms of isoform-specific PI3K signalling. *Nat. Rev. Mol. Cell Biol.* **11**, 329-341 (2010).
628 34. Tessier, M. & Woodgett, J. Serum and glucocorticoid-regulated protein kinases: Variations on a
629 theme. *J. Cell Biochem.* **98**, 1391–1407 (2006).
630 35. Kobayashi, T., Deak, M., Morrice, N. & Cohen, P. Characterization of the structure and
631 regulation of two novel isoforms of serum- and glucocorticoid-induced protein kinase. *Biochem.*
632 *J.* **344**, 189–197 (1999).
633 36. Malik, N. et al. Mechanism of activation of SGK3 by growth factors via the Class 1 and Class 3
634 PI3Ks. *Biochem. J.* **475,** 117–135 (2018).
635 37. Pearce, L., Komander, D. & Alessi, D. The nuts and bolts of AGC protein kinases. *Nat. Rev.*
636 *Mol. Cell Biol.* **11**, 9–22 (2010).
637 38. Kobayashi, T. & Cohen, P. Activation of serum- and glucocorticoid-regulated protein kinase by
638 agonists that activate phosphatidylinositide 3-kinase is mediated by 3-phosphoinositide-dependent
639 protein kinase-1 (PDK1) and PDK2. *Biochem. J.* **339**, 319–328 (1999).
640 39. Tessier, M. & Woodgett, J. R. Role of the Phox homology domain and phosphorylation in
641 activation of serum and glucocorticoid-regulated kinase-3. *J. Biol. Chem.* **281**, 23978–23989 (2006).
642 40. García-Martínez, J. M. & Alessi, D. R. mTOR complex 2 (mTORC2) controls hydrophobic
643 motif phosphorylation and activation of serum- and glucocorticoid-induced protein kinase 1 (SGK1).
644 *Biochem. J.* **416**, 375–385 (2008).
645 41. Biondi, RM., Kieloch, A., Currie, RA., Deak, M. & Alessi, DR. The PIF-binding pocket in
646 PDK1 is essential for activation of S6K and SGK, but not PKB. *EMBO J.* **20**, 4380-4390 (2001).

647 42. Lu, M. et al. mTOR Complex-2 Activates ENaC by Phosphorylating SGK1. *J. Am. Soc.*
648 *Nephrol.* **21,** 811–818 (2010).
649 43. Lien, E. C., Dibble, C. C. & Toker, A. PI3K signaling in cancer: beyond AKT. *Curr. Opin. Cell*
650 *Biol.* **45**, 62–71 (2017).
651 44. Hiraoka, D. et al. PDK1 is required for the hormonal signaling pathway leading to meiotic
652 resumption in starfish oocytes. *Dev. Biol.* **276**, 330–336 (2004).
653 45. Hiraoka, Okumura & Kishimoto, T. Turn motif phosphorylation negatively regulates activation
654 loop phosphorylation in Akt. *Oncogene* **30**, 4487–4497 (2011).
655 46. Okumura, E. et al. Akt inhibits Myt1 in the signalling pathway that leads to meiotic
656 G2/M-phase transition. *Nat. Cell. Biol.* **4**, 111–116 (2002).
657 47. Okumura, E., Sekiai, T., Hisanaga, S., Tachibana, K. & Kishimoto, T. Initial triggering of
658 M-phase in starfish oocytes: a possible novel component of maturation-promoting factor besides
659 cdc2 kinase. *J. Cell Biol.* **132**, 125–135 (1996).
660 48. Eltschinger, S. & Loewith, R. TOR complexes and the maintenance of cellular
661 homeostasis. *Trends Cell Biol.* **26**, 148–159 (2016).
662 49. Kinoshita, E., Kinoshita-Kikuta, E., Takiyama, K. & Koike, T. Phosphate-binding Tag, a New
663 Tool to Visualize Phosphorylated Proteins. *Mol. Cell Proteomics* **5,**749–757 (2006).
664 50. Miyazaki, S. & Hirai, S. Fast polyspermy block and activation potential correlated changes
665 during oocyte maturation of a starfish. *Dev. Biol.* **70**, 327–340 (1979).
666 51. Hayashi, M. et al. BMK1 mediates growth factor-induced cell proliferation through direct
667 cellular activation of SGK. *J. Biol. Chem.* **276**, 8631–8634 (2001).
668 52. Gasser, J. et al. SGK3 mediates INPP4B-dependent PI3K signaling in breast cancer. *Mol.*
669 *Cell* **56**, 595–607 (2014).

670 53. Hiraoka, D., Hosoda, E., Chiba, K. & Kishimoto, T. SGK phosphorylates Cdc25 and Myt1 to
671 trigger cyclin B-Cdk1 activation at the meiotic G2/M transition. Preprint at
672 https://doi.org/10.1101/499640 (2018).
673 54. Terasaki, M. et al. A new model for nuclear envelope breakdown. *Mol. Biol. Cell* **12**, 503–510
674 (2001).
675 55. Lénárt, P. et al. Nuclear envelope breakdown in starfish oocytes proceeds by partial NPC
676 disassembly followed by a rapidly spreading fenestration of nuclear membranes. *J. Cell*
677 *Biol.* **160**, 1055–1068 (2003).
678 56. Mori, M. et al. An Arp2/3 nucleated F-actin shell fragments nuclear membranes at nuclear
679 envelope breakdown in starfish oocytes. *Curr. Bio.* **24**, 1421–1428 (2014).
680 57. Jenkins, E., Debnath, S., Varriano, S., Gundry, S. & Fata, J. Na^+/H^+ exchanger 1 (NHE1)
681 function is necessary for maintaining mammary tissue architecture. *Dev. Dyn.* **243**, 229–242 (2014).
682 58. Rodeau, J. L. & Vilain, J. P. Changes in membrane potential, membrane resistance, and
683 intracellular H^+, K^+, Na^+, and Cl^- activities during the progesterone-induced maturation of urodele
684 amphibian oocytes. *Dev. Biol.* **120**, 481–493 (1987).
685 59. Stith, B. & Maller, J. Increased intracellular pH is not necessary for ribosomal protein S6
686 phosphorylation, increased protein synthesis, or germinal vesicle breakdown in Xenopus
687 oocytes. *Dev. Biol.* **107**, 460–469 (1985).
688 60. Sellier, C. *et al.* Intracellular acidification delays hormonal G2/M transition and inhibits G2/M
689 transition triggered by thiophosphorylated MAPK in Xenopus oocytes. *J. Cell Biochem.* **98,** 287–300
690 (2006).
691 61. Tachibana, K., Machida, T., Nomura, Y. & Kishimoto, T. MAP kinase links the fertilization
692 signal transduction pathway to the G1/S-phase transition in starfish eggs. *EMBO J.* **16**, 4333–4339
693 (1997).

694 62. Tachibana, K., Tanaka, D., Isobe, T. & Kishimoto, T. c-Mos forces the mitotic cell cycle to
695 undergo meiosis II to produce haploid gametes. *Proc. Natl. Acad. Sci. USA* **97**, 14301-14306 (2000).
696 63. Flament, S., Browaeys, E., Rodeau, J. L., Bertout, M. & Vilain, J. P. Xenopus oocyte
697 maturation: cytoplasm alkalization is involved in germinal vesicle migration. *Int. J. Dev.*
698 *Biol.* **40**, 471–476 (1996).
699 64. Kishimoto, T. Microinjection and cytoplasmic transfer in starfish oocytes. *Methods Cell Biol.*
700 **27**, 379-394 (1986).
701 65. Chiba, K. *et al.* The primary structure of the α subunit of a starfish guanosine-nucleotide-
702 binding regulatory protein involved in 1-methyladenine-induced oocyte maturation. *Eur. J.*
703 *Biochem.* **207**, 833–838 (1992).
704 66. Hamaguchi, M., Watanabe, K. & Hamaguchi, Y. Regulation of intracellular pH in sea urchin
705 eggs by medium containing both weak acid and base. *Cell Struct. Funct.* **22**, 387–398 (1997).
706 67. Hijikata, A., Yura, K., Noguti, T. & Go, M. Revisiting gap locations in amino acid sequence
707 alignments and a proposal for a method to improve them by introducing solvent
708 accessibility. *Proteins* **79**, 1868–1877 (2011).

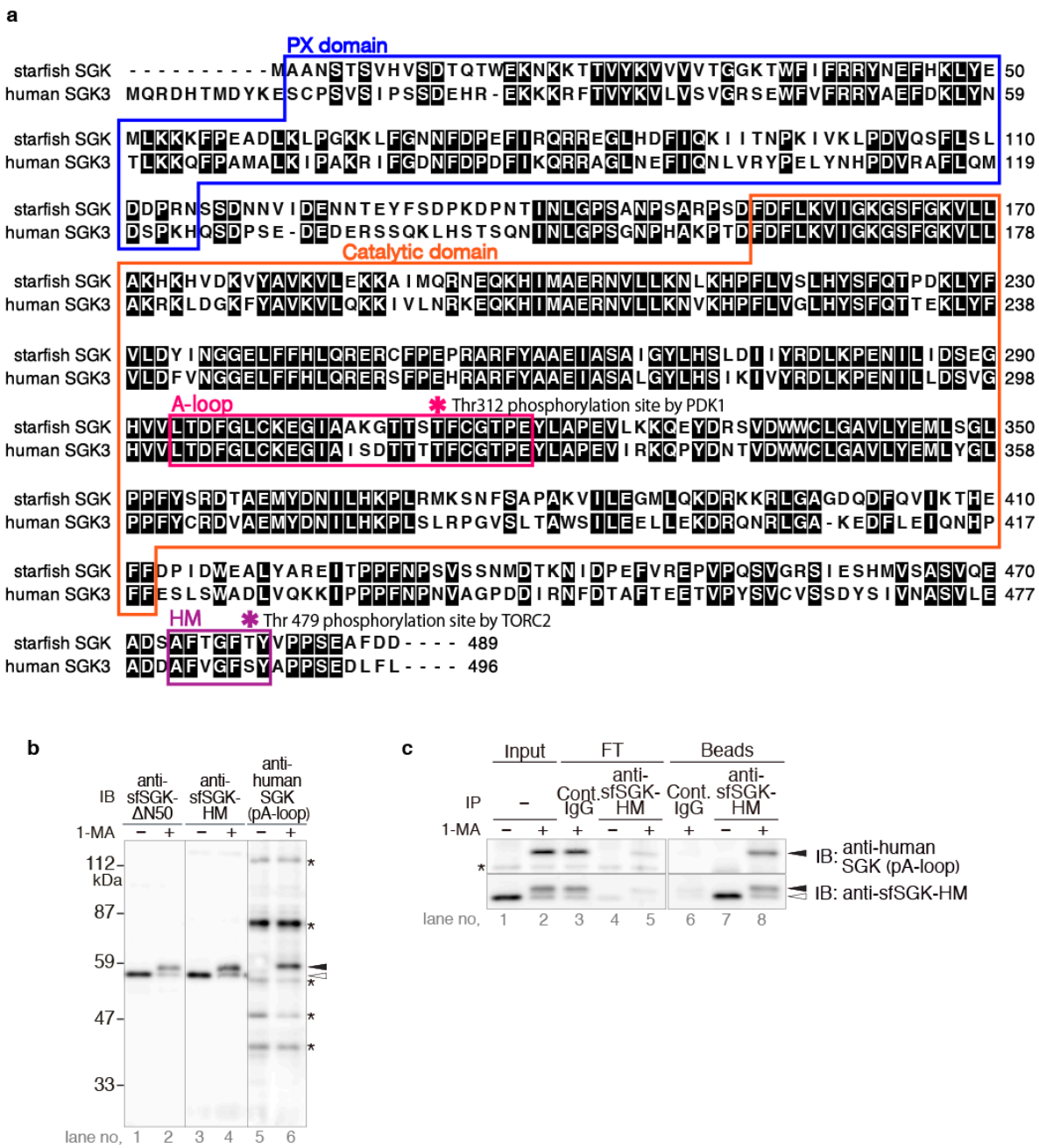

Figure 1 sfSGK protein and phosphorylation of its A-loop are detectable in starfish oocytes.

a The deduced amino acid sequence of starfish SGK (sfSGK) was aligned with that of human SGK3 (NCBI accession number NP_001028750.1) using the ALAdeGAP alignment software[67]. The sfSGK sequence has been submitted to the DDBJ/EMBL/Gen Bank databases under accession number LC430700. Identical amino acids are shaded. Dashes indicate gaps introduced for optimal alignment. Colored boxes indicate conserved domains: PX domain (blue), Activation-loop (A-loop; magenta), Hydrophobic motif (HM; purple), and Catalytic domain (orange). Magenta and purple asterisk indicate conserved residues phosphorylated by PDK1 (Thr312 in starfish; Thr320 in human) and TORC2 (Thr479 in starfish: Ser486 in human), respectively. **b** Unstimulated starfish oocytes were incubated with or without 1-MA for 4 min, followed by immunoblotting with anti-sfSGK-ΔN50,

720 anti-sfSGK-HM, and anti-human phospho-SGK (anti-human SGK [pA-loop]) antibodies. Asterisks
721 indicate non-specific bands. The result shown is representative of three independent experiments. **c**
722 Immunoprecipitation (IP) was performed with anti-sfSGK-HM antibody or control IgG using
723 extracts prepared from unstimulated or 1-MA stimulated oocytes. Input extract (Input), flow-through
724 (FT), and beads (Beads) samples were analyzed by immunoblotting with the indicated antibodies
725 (IB). Asterisk indicates non-specific bands detected by anti-human phospho-SGK (anti-human SGK
726 [pA-loop]). The indicated result is representative of two independent experiments. Closed and open
727 arrowheads indicate positions of the upper and lower bands of sfSGK, respectively (**b**, **c**).

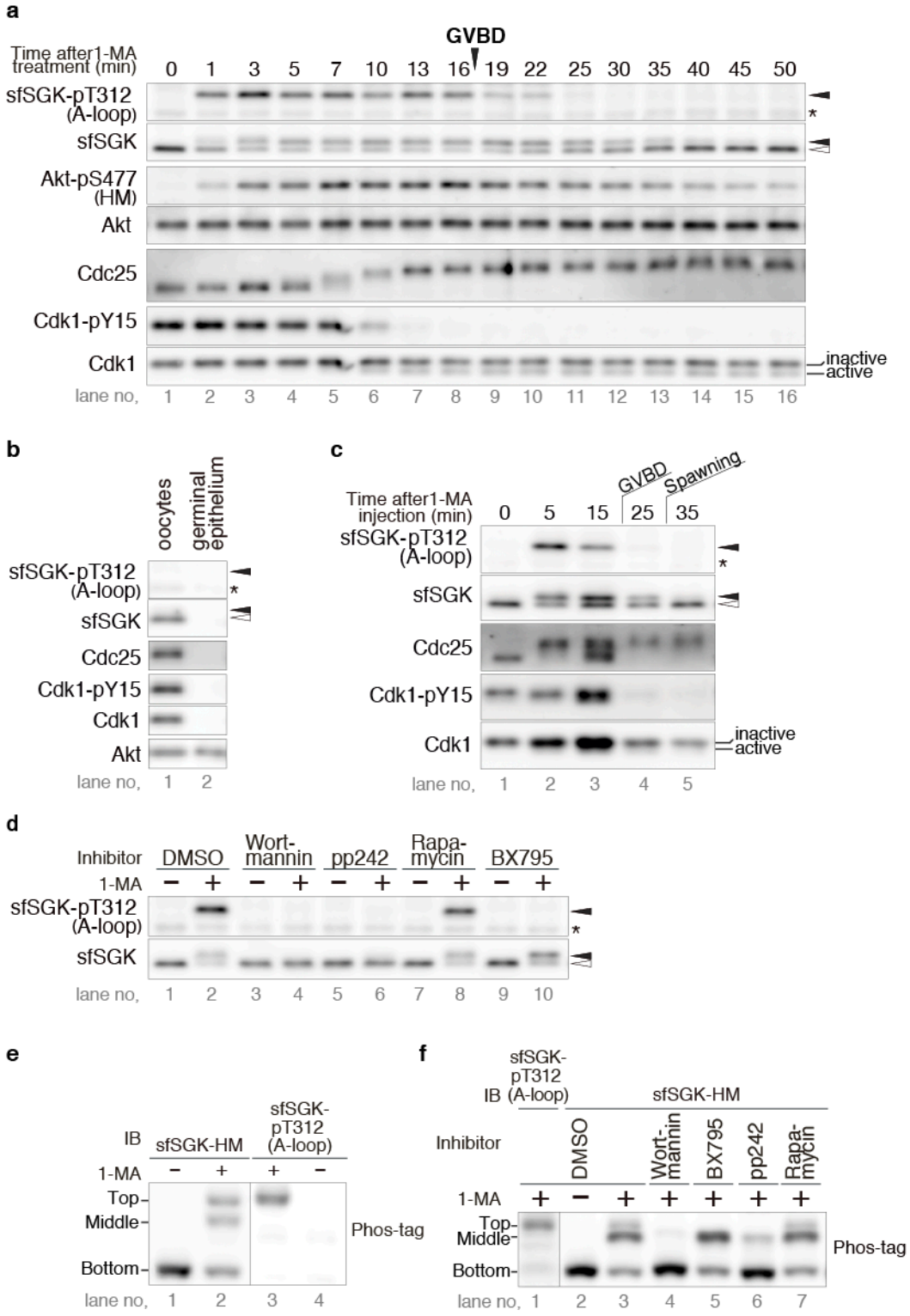

728

729 **Figure 2 sfSGK is activated by PDK1 and TORC2 in a PI3K-dependent manner.**

730 **a** Isolated oocytes were treated with 1-MA and recovered at the indicated times, followed by
731 immunoblotting with anti-human phospho-SGK (sfSGK-pT312 [A-loop]), anti-sfSGK-HM (sfSGK),
732 anti-starfish phospho-Akt-HM (Akt-pS477[HM]), anti-starfish Akt C-terminal fragment (Akt),

733 anti-starfish Cdc25 (Cdc25), anti-phospho-Cdk1 (Cdk1-pY15), and anti-PSTAIR (Cdk1) antibodies.
734 GVBD occurred at 17 min. The result shown is representative of three independent experiments. **b** A
735 piece of ovary was taken from female starfish, separated into oocytes and germinal epithelium, and
736 subjected to immunoblotting with indicated antibodies. **c** To stimulate ovarian oocytes, 1-MA was
737 injected into the body cavity of female starfish, and then two pieces of ovaries were recovered at
738 indicated times. One piece of ovary was immediately added to sample buffer for immunoblotting
739 with the indicated antibodies. Oocytes from the other piece of the ovary were monitored to count
740 GVBD. GVBD occurred within 25 min, and spawning started at 30 min. The result shown is
741 representative of two independent experiments. **d** Isolated oocytes were treated with 1-MA for 4 min
742 in the presence of indicated inhibitors or DMSO, and then subjected to normal SDS-PAGE, followed
743 by immunoblotting with the indicated antibodies. The result shown is representative of two
744 independent experiments. **e** Isolated oocytes were treated with 1-MA for 4 min, and then subjected to
745 Phos-tag SDS-PAGE, followed by immunoblotting with the indicated antibodies (IB). The result
746 shown is representative of three independent experiments. **f** Isolated oocytes were treated with 1-MA
747 for 4 min in the presence of indicated inhibitors, and subjected to Phos-tag SDS PAGE, followed by
748 immunoblotting with the indicated antibodies (IB). The result shown is representative of three
749 independent experiments. Closed and open arrowheads indicate positions of the upper and lower
750 band of sfSGK, respectively (**a**, **b, c** and **d**). Asterisks indicate non-specific bands (**a**, **b**, **c,** and **d**).

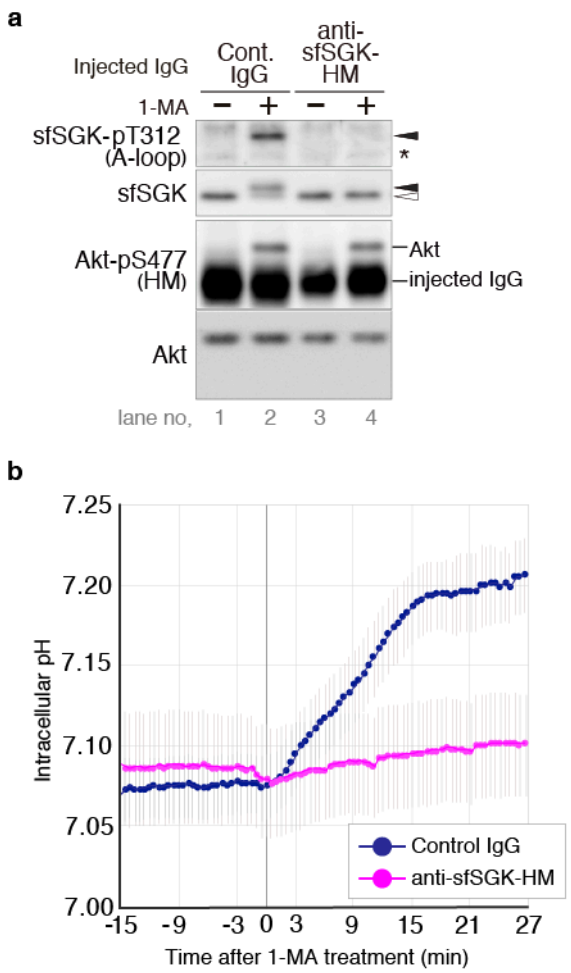

Figure 3 Activation of sfSGK is required for rapid pH_i increase after 1-MA stimulus.

a Unstimulated oocytes were injected with an anti-sfSGK-HM antibody or control IgG, treated with 1-MA for 4 min, and then subjected to immunoblotting with indicated antibodies. Asterisk indicates non-specific bands. Closed and open arrowheads indicate positions of the upper and lower band of sfSGK, respectively. The result shown is representative of three independent experiments. **b** BCECF-dextran and either anti-sfSGK-HM antibody or control IgG were co-injected into unstimulated oocytes. After a 1-h incubation, 1-MA was added, and the fluorescence intensity ratio was measured every 30 seconds before and after 1-MA addition. pH_i was calculated from the fluorescence intensity ratio and plotted. Data represent means ± SE of three independent experiments.

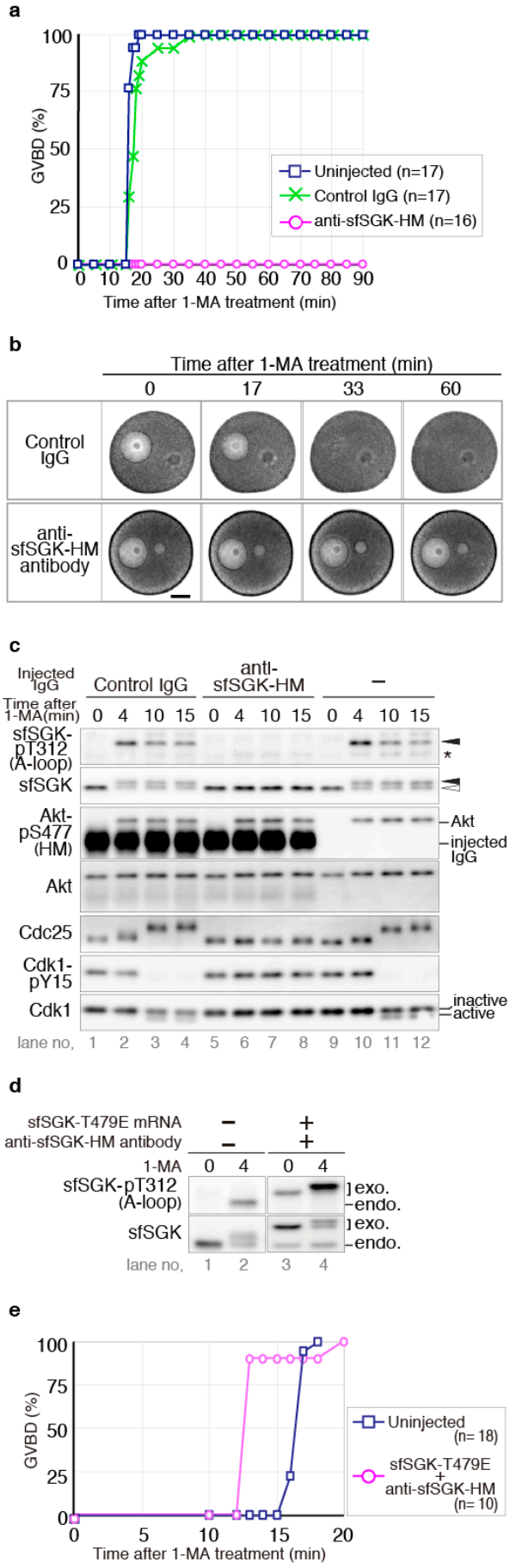
a
GVBD (%)
Time after 1-MA treatment (min)
Uninjected (n=17)
Control IgG (n=17)
anti-sfSGK-HM (n=16)
b
Time after 1-MA treatment (min)
0
17
33
60
Control IgG
anti-sfSGK-HM antibody
c
Injected IgG
Control IgG
anti-sfSGK-HM
–
Time after 1-MA(min)
sfSGK-pT312 (A-loop)
sfSGK
Akt-pS477 (HM)
Akt
injected IgG
Cdc25
Cdk1-pY15
Cdk1
inactive
active
lane no,
d
sfSGK-T479E mRNA
anti-sfSGK-HM antibody
1-MA
sfSGK-pT312 (A-loop)
sfSGK
exo.
endo.
lane no,
e
GVBD (%)
Time after 1-MA treatment (min)
Uninjected (n= 18)
sfSGK-T479E + anti-sfSGK-HM (n= 10)

762

763 **Figure 4 Activation of sfSGK is required for cyclin B–Cdk1 activation.**

764 **a**–**c** Unstimulated oocytes were injected with anti-sfSGK-HM antibody or control IgG, treated with
765 1-MA, and subjected to the following experiments: monitoring of GVBD (**a**), imaging by differential
766 interference contrast (DIC) microscopy (**b**), and immunoblotting with the indicated antibodies (**c**) at
767 the indicated times. "n" indicates the number of oocytes observed (**a**). An oil drop, that had been
768 introduced along with the antibodies as a mark of the microinjection, was observed on the right of
769 the GV (**b**). Scale bar represents 50 μm (**b**). Asterisk indicates a non-specific band (**c**). Closed and
770 open arrowheads indicate positions of the upper band and the lower band of sfSGK, respectively (**c**).
771 Results are representative of two independent experiments. **d**, **e** Anti-sfSGK-HM antibody was
772 injected into unstimulated oocytes. After incubation for 1 h, mRNA encoding a mutant sfSGK
773 (T479E) was injected into the same oocytes, followed by incubation for 17 h. As a control,
774 uninjected oocytes were incubated for 17 h. These oocytes were treated with 1-MA, followed by
775 immunoblotting with indicated antibodies (**d**) and counting of GVBD (**e**) at the indicated times. "exo."
776 and "endo." indicate exogenous and endogenous sfSGK, respectively (**d**). "n" indicates the number
777 of oocytes observed (**e**). Results are representative of two independent experiments.

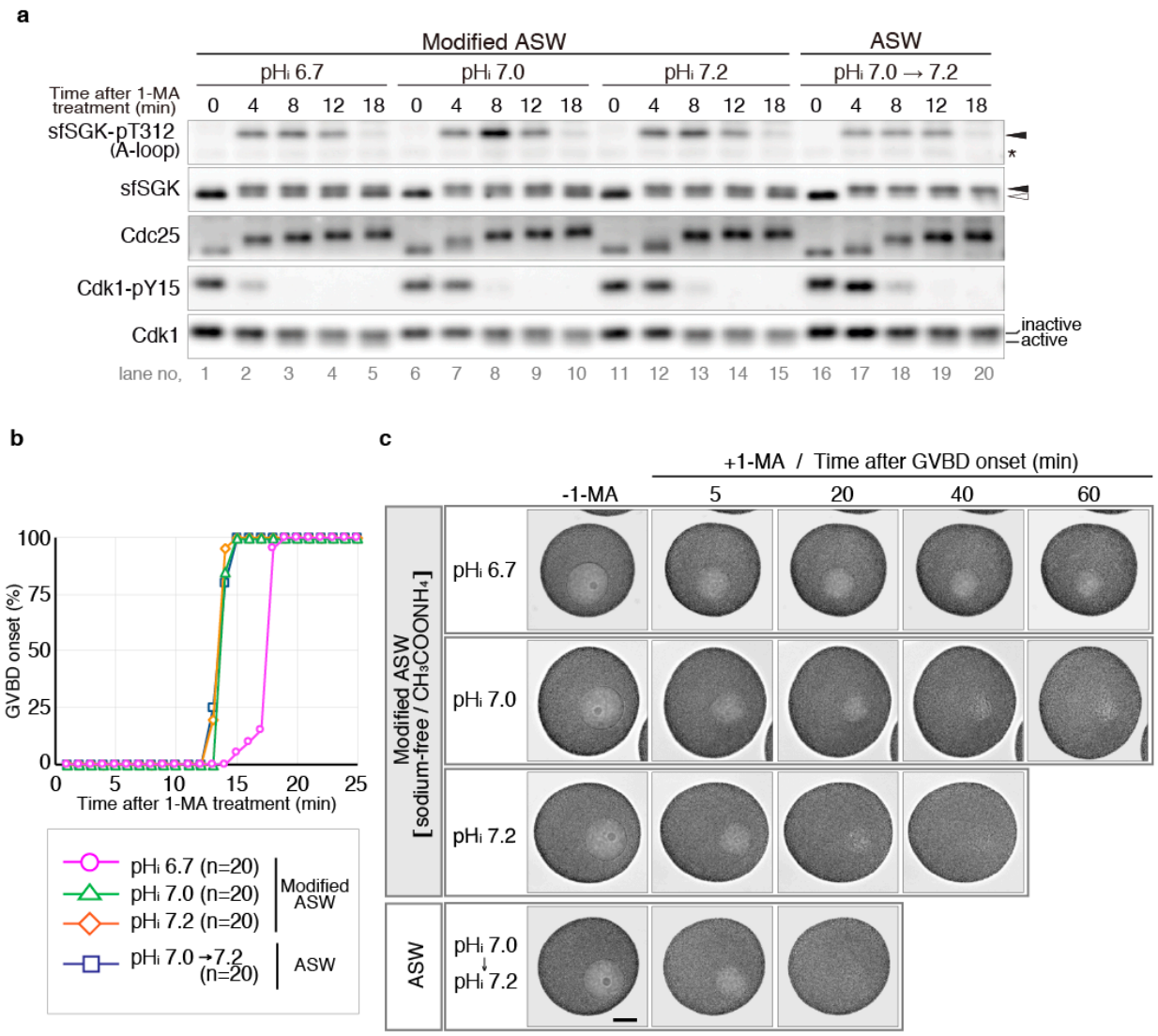

Figure 5 Reduced pH_i delays onset of GVBD and blocks completion of GVBD without affecting cyclin B–Cdk1 activation.

a To clamp pH_i at 6.7, 7.0, and 7.2, unstimulated oocytes were incubated with sodium-free artificial seawater containing CH_3COONH_4 (Modified ASW) for 20 min. As a control, unstimulated oocytes were incubated in artificial seawater (ASW) for 20 min, in which pH_i is approximately 7.0, and increases to ~7.2 after 1-MA treatment[17] (see also control IgG–injected oocytes in Fig. 3b). These oocytes were treated with 1-MA and analyzed by immunoblotting with indicated antibodies. Asterisk indicates a non-specific band. Closed and open arrowheads indicate the positions of the upper and lower bands of sfSGK, respectively. **b** Oocytes treated as described in **a** were monitored to count onset of GVBD. "n" indicates the number of oocytes observed. Morphology of GVBD onset is shown in Supplementary Fig. 2. **c** Time-lapse DIC images of oocytes treated as described in **a** were taken every 10 seconds before and after addition of 1-MA. Images at selected times after GVBD onset are shown. Scale bar represents 50 µm. For complete image sequences, see Supplementary movies 1–4. For Z-stack images acquired after the time-lapse imaging, see Supplementary Fig. 3. Results in all panels are representative of two independent experiments.

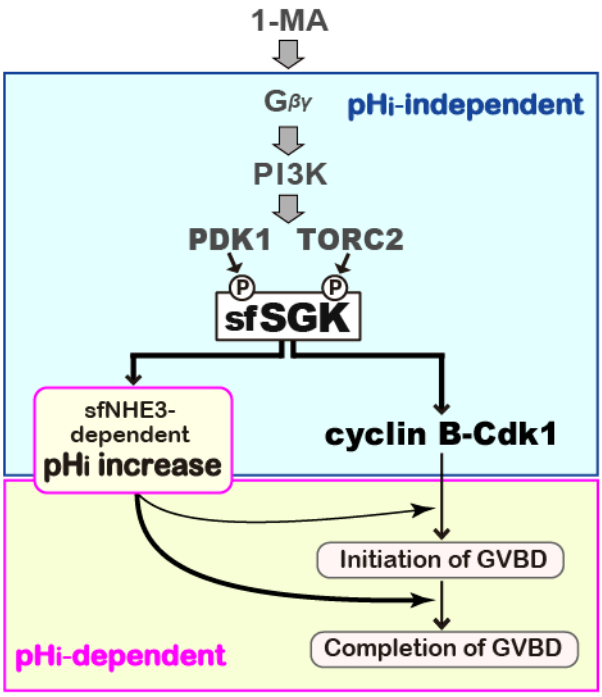

Figure 6 Model for sfSGK-dependent meiotic resumption: sfSGK induces cyclin B–Cdk1 activation to resume meiosis and pH_i increase to complete GVBD in ovarian oocytes.
A model for 1-MA–induced meiotic resumption in ovarian oocytes was prepared on the basis of previous and current findings. 1-MA stimulus induces the release of Gβγ from Gαi, leading to PI3K activation. In a manner that depends on PI3K, sfSGK is activated via phosphorylation of the A-loop by PDK1 after prior phosphorylation of the HM by TORC2. Activation of sfSGK is essential for cyclin B–Cdk1 activation and sfNHE3-dependent pH_i increase. These SGK-dependent pathways are pH_i-independent (blue box). On the other hand, time to GVBD onset after cyclin B–Cdk1 activation and completion of GVBD are pH_i-dependent (yellow box), and both are defective at pH_i of 6.7. Because pH_i of ovarian oocytes before 1-MA stimulation in body cavity is ~6.7, the sfSGK-dependent pH_i increase after 1-MA stimulus accelerates GVBD onset and is required for completion of GVBD in ovarian oocytes. By contrast, the pH_i of isolated oocytes before 1-MA stimulation in ASW is ~7.0, which is already permissive for GVBD. Therefore, a pH_i increase is not essential for GVBD in isolated oocytes.